JACS
JOURNAL OF THE AMERICAN CHEMICAL SOCIETY

ARTICLE

pubs.acs.org/JACS

Fabrication of Asymmetric Molecular Junctions by the Oriented Assembly of Dithiocarbamate Rectifiers

Deqing Gao,[†] Frank Scholz,[†] Heinz-Georg Nothofer,[†] William E. Ford,[†] Ullrich Scherf,[§] Jurina M. Wessels,[†] Akio Yasuda,[†] and Florian von Wrochem*[,†]

[†]Sony Deutschland GmbH, Materials Science Laboratory, Hedelfinger Strasse 61, 70327 Stuttgart, Germany

[§]Bergische Universität Wuppertal, Makromolekulare Chemie und Institut für Polymertechnologie, Gauss-Strasse 20, 42097 Wuppertal, Germany

Supporting Information

ABSTRACT: The oriented assembly of molecules on metals is a requirement for rectification in planar metal−molecule−metal junctions. Here, we demonstrate how the difference in adsorption kinetics between dithiocarbamate and thioacetate anchor groups can be utilized to form oriented assemblies of asymmetric molecules that are bound to Au through the dithiocarbamate moiety. The free thioactate group is then used as a ligand to bind Au nanoparticles and to form the desired metal−molecule−metal junction. Besides allowing an asymmetric coupling to the electrodes, the molecules exhibit an asymmetric molecular backbone where the length of the alkyl chains separating the electrodes from a central, *para*-substituted phenyl ring differs by two methylene units. Throughout the junction fabrication, the layers were characterized by photoelectron spectroscopy, infrared spectroscopy, and scanning tunneling microscopy. Large area junctions using a conducting polymer interlayer between a mercury-drop electrode and the self-assembled monolayer prove the relationship between electrical data and molecular structure.

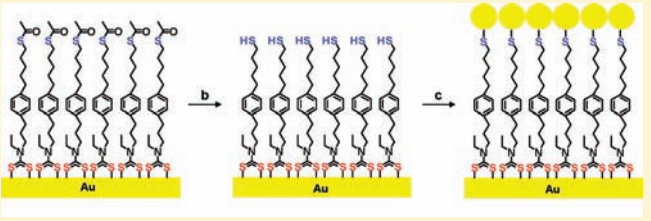

INTRODUCTION

The physical limits encountered in the miniaturization of CMOS devices and the exponential increase in the production cost of future CMOS-based electronics[1] have triggered a growing research effort in the area of molecular electronics.[2−4] Consequently, the development of concepts and experimental test-beds for the implementation of organic molecules in electronic devices has attracted significant interest.[5] For the realization of organic-based memories[6,7] and field-programmable gate arrays,[8] the development of molecular rectifiers is an issue of fundamental importance. By definition, a rectifier (diode) is a two-terminal device with a unipolar current−voltage characteristic. The first concept of a unipolar molecular diode, based on a donor-insulator-acceptor (D-σ-A) model, was proposed by Aviram and Ratner.[9] According to this model, a recombination of opposite charges previously transferred from the electrodes into the highest occupied molecular orbital (HOMO) and the lowest unoccupied molecular orbital (LUMO) of two decoupled units within the rectifier (D^+-σ-A^- zwitterion state) takes place.[10] Williams et al. described a different mechanism for molecular rectification where a single electroactive unit (e.g., a phenyl ring) is asymmetrically positioned between two electrodes.[11] In this case, the alignment of the HOMO and LUMO of the phenyl ring with the Fermi levels of the contacts determines the asymmetry of the current−voltage characteristics, and rectification ratios of up to 500 were predicted by appropriately tuning the tunneling barrier lengths, which are given by two insulating alkyl chains.[11]

For the fabrication of lithographically defined, micrometer- to nanometer-scale (μm- to nm-scale) molecular junctions, the formation of ultrathin self-assembled monolayers in a solution deposition process is one of the most promising assembly strategies.[7,12,13] However, the realization of diodic junctions featuring a well-defined electrical response requires an oriented growth of asymmetric molecules at metal surfaces.[14] Moreover, a well-defined packing density and tilt angle of the molecular backbone within the monolayer are essential to obtain reproducible current−voltage characteristics. Recently, the oriented growth of asymmetric molecules on noble metals has been achieved with dithiols having different, orthogonal protective groups, such as trimethylsilylethyl,[15] acetyl,[16] and cyanoethyl.[14] These protective groups can be removed sequentially, allowing selective binding to the substrate via the desired thiolate end group. Nevertheless, the synthesis of such asymmetrically protected dithiol derivatives is demanding, and processing conditions for the sequential removal of orthogonal protective groups have to be accurately controlled. Furthermore, no asymmetry in the electrical coupling to the electrodes is possible if thiolates are used on both sides of the junction.

An alternative pathway for the directional assembly at surfaces is the usage of two different anchor groups. In the past, dithiocarbamate anchor groups have been investigated in

Received: November 15, 2010
Published: March 28, 2011

dx.doi.org/10.1021/ja110244j | *J. Am. Chem. Soc.* 2011, 133, 5921–5930

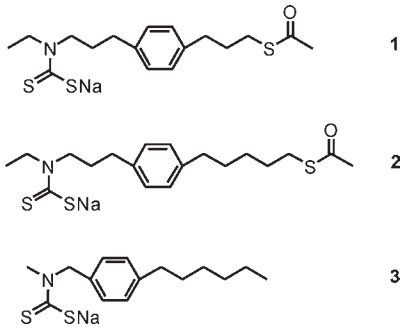

Figure 1. Molecular structures of dithiocarbamate/thiol compounds **1** and **2** and of compound **3**, which was used as a reference in this study.

metal−nanoparticle networks[17] and self-assembled monolayers.[18−22] It has been shown experimentally[22] and theoretically[22,23] that the conjugated dithiocarbamate anchor group strongly couples to coinage metals, causing a mixing of discrete molecular levels with metal states, thereby leading to a significant reduction of the metal−molecule charge injection barrier. This results in a lower contact resistance than thiols at the metal−molecule interface. Furthermore, it was shown that dithiocarbamate monolayers are thermally more stable than comparable thiolate monolayers.[22]

In this paper, we target the fabrication of monolayer-based rectifier junctions using molecules having two different anchor groups. On one hand, this enables a directional molecular assembly on metal surfaces. On the other hand, an asymmetric electrical coupling to the electrodes is possible. On the basis of the theoretical work of Williams et al.,[11] we designed and synthesized two asymmetric compounds, **1** and **2** (Figure 1), having a central phenyl ring and two alkyl chains in the *para*-positions as insulating barriers. Whereas derivative **1** has an *n*-propyl chain on each side, **2** contains an *n*-propyl chain and *n*-pentyl chain at the two *para* positions of the phenyl ring, thus being also asymmetric in terms of tunneling barrier length. Instead of two identical thiol-based anchor groups,[11] the present derivatives contain a dithiocarbamate (NCS_2) and an acetyl protected thiol group ($SCOCH_3$), respectively. The difference in length of the two tunneling barriers separating the central phenyl ring from the electrodes and the combination of different anchor groups connecting the molecule with the leads has shown to dramatically increase rectification.[24] The dithiocarbamate group is a strong chelating agent,[25] and reacts faster with the Au surface than the acetyl protected thiol.[26,27] As a result, an oriented monolayer was obtained. Subsequent removal of the acetyl protective groups allowed the reaction of Au nanoparticles from solution with the thiol surface for top electrode formation in a mild deposition step. With this procedure, a simple way of realizing an asymmetric metal−molecule−metal junction without using different thiol protective groups is disclosed. The whole process, that is, monolayer formation, deprotection, and nanoparticle growth, was monitored by X-ray photoelectron spectroscopy (XPS), polarization modulation infrared reflection−absorption spectroscopy (PM-IRRAS), scanning tunneling microscopy (STM), and contact angle goniometry. The electrical properties of asymmetric molecular junctions were determined using a polymeric interlayer between a liquid top electrode and the oriented self-assembled monolayer.

RESULTS AND DISCUSSION

Synthesis and Characterization. The syntheses of compounds **1** and **2** are depicted in Scheme 1. 3-Phenyl-1-propylamine was reacted with acetic anhydride to give amide **4** which was then used as starting material for the synthesis of **1** and **2**. Compounds **5** and **6** were prepared by Friedel−Crafts acylation of **4**. Borane is known as a good reducing agent for amides without reacting with halides.[28] First, borane-tetrahydrofuran ($BH_3 \cdot THF$) was chosen to carry out the reduction of the two ketone groups of **5** or **6**. However, characterization of the resulting products by ^1H NMR analysis showed that, in case of both compounds, the amide group was reduced to amine, whereas the carbonyl group next to the aryl was only reduced to alcohol. Thus, a two-step reduction was carried out. In the first step, triethylsilane (Et_3SiH) in trifluoroacetic acid (TFA)[29] was used to reduce the aryl ketone to methylene in high yield. In a second step, the amide was reduced to amine by using borane-dimethyl sulfide (BMS, $BH_3 \cdot S(CH_3)_2$), which is easier to handle than $BH_3 \cdot THF$.[30] The products **9** and **10** were then subjected to nucleophilic substitution by reacting with potassium thioacetate[31] in the presence of sodium iodide as the halide-exchange agent. A slow addition of potassium thioacetate was necessary to prevent β-elimination of HCl as a competing reaction. The acetyl-protected thiol compounds **11** and **12** were treated with carbon disulfide and sodium methoxide resulting in the corresponding dithiocarbamate salts **1** and **2**.

The synthesis of compound **3** is depicted in Scheme 2. Trifluoroacetyl was selected to protect the amine group of *N*-methyl benzylamine because it can be removed more easily than the acetyl group. Thus, *N*-methyl benzylamine was first acetylated with trifluoroacetic anhydride.[32] Through a stepwise Friedel−Crafts acylation, reduction of the aryl ketone, and deprotection of the trifluoroacetyl group, the amine **16** was obtained. In a subsequent reaction, compound **16** was treated with carbon disulfide and sodium methoxide, yielding the dithiocarbamate salt **3**. It is worth noting that the reduction of compound **14** followed by the deprotection[33] of **15** was successful, whereas the reverse procedure was not. This might be due to deactivation of the reducing agent by the amine. Further details concerning the syntheses and characterization of **1**−**3** can be found in the Supporting Information.

Junction Fabrication. A sequence of steps is required to realize asymmetric molecular junctions within a "bottom-up" assembly strategy, and in each of these steps, different analysis techniques provide the necessary information about surface chemistry and layer structure. Photoelectron spectroscopy, infrared spectroscopy, scanning probe microscopy, and contact angle goniometry were employed, yielding information on monolayer and electrode structure, binding chemistry at the interface, and molecular orientation.

The junction fabrication can be divided into three main processing steps: (a) oriented monolayer formation in a self-assembly process, (b) deprotection of the exposed thiol end groups, and (c) gold nanoparticle (NP) deposition for electrode formation. The scheme in Figure 2 shows these steps with the asymmetric rectifier **2** as an example.

Monolayer Formation. The adsorption of dithiocarbamates to Au was first studied using a simple compound (**3**, see Figure 1) whose structure is closely related to **1** and **2**, but lacking the terminal thiol group. It further has a methyl substituent rather than an ethyl substituent on the dithiocarbamate anchor group. Compound **3** was selected as a reference because the interaction of the molecule with the substrate is reduced to the dithiocarbamate anchor group only, excluding any additional influence/interaction arising from the thioacetate moiety during self-assembly.

Scheme 1. Synthesis of Compounds 1 and 2[a]

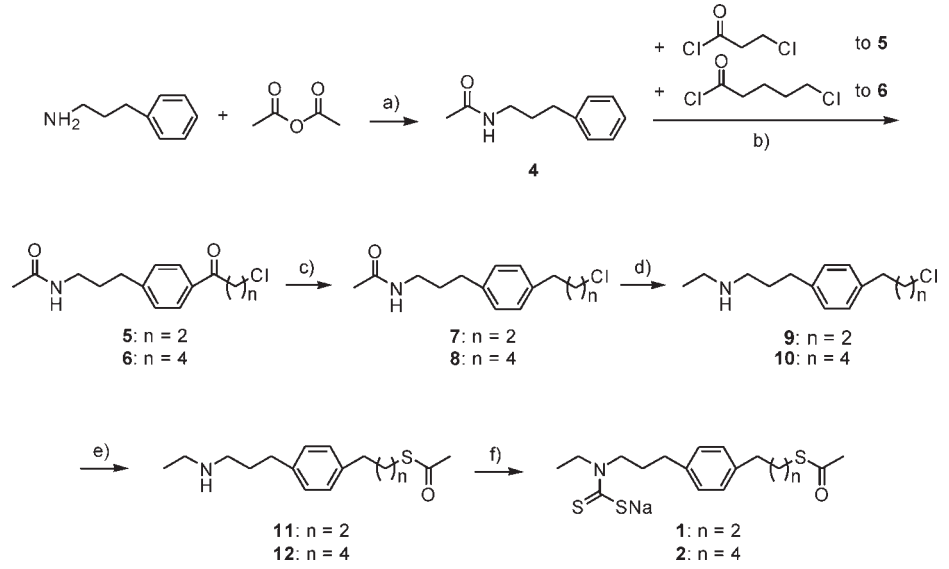

[a] Conditions: (a) AcOH, heating; (b) $AlCl_3$, CS_2, r.t.; (c) Et_3SiH, TFA, r.t.; (d) $BH_3 \cdot S(CH_3)_2$, THF, reflux; (e) $KSCOCH_3$, NaI, DMF, r.t.; (f) NaOMe, CS_2, $CHCl_3$, r.t.

Scheme 2. Synthesis of Compound 3[a]

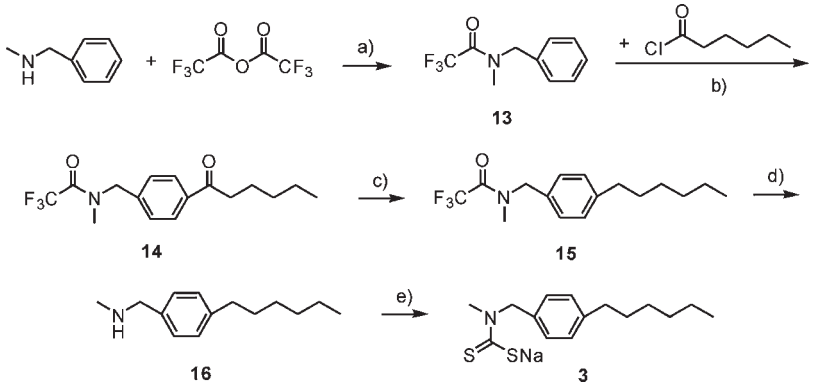

[a] Conditions: (a) diethyl ether, r.t.; (b) $AlCl_3$, CS_2, reflux; (c) Et_3SiH, TFA, r.t.; (d) K_2CO_3, CH_3OH/H_2O, r.t.; (e) NaOMe, CS_2, $CHCl_3$, r.t.

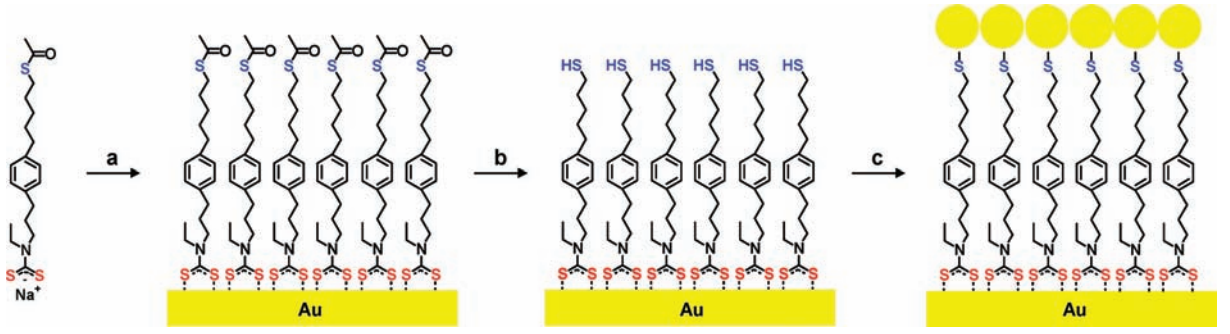

Figure 2. Schematic illustration of the fabrication steps for the formation of asymmetric metal−monolayer−metal junctions using compound **2**: (a) self-assembly on Au; (b) deprotection; (c) deposition of Au nanoparticles by incubation.

The adsorption characteristics of **3** to the Au substrate are accessible through X-ray photoelectron spectroscopy in the S 2p core level region (Figure 3), which shows a unique signal (S $2p_{3/2}$/S $2p_{1/2}$ peak doublet) attributed to chemisorbed sulfur (161.94 eV)[34] at binding energies consistent with reported values for dialkyl dithiocarbamates on Au[18] and slightly lower

dx.doi.org/10.1021/ja110244j |*J. Am. Chem. Soc.* 2011, 133, 5921–5930

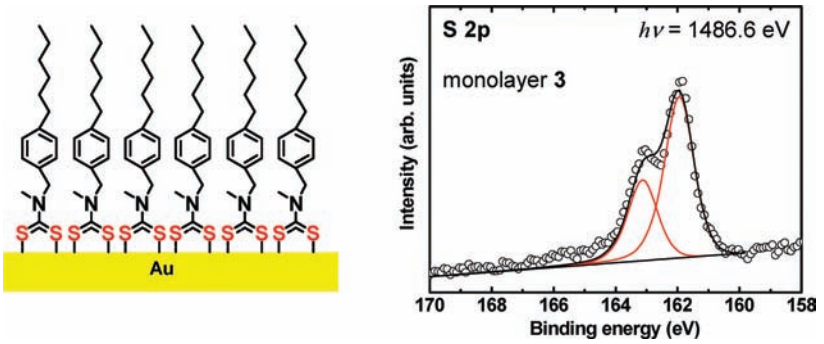

Figure 3. XP spectrum of monolayer **3** on Au(111), showing a S $2p_{3/2}$ core-level peak at 161.94 eV. A single component (S $2p_{3/2}$/S $2p_{1/2}$ doublet) appeared, representative of the bidentate bond of the dithiocarbamate moiety to Au. Single fit curves to the data are drawn in red; the sum of the fit curves and the linear background are drawn in black. The scheme on the left shows the molecular arrangement of **3** on Au.

Table 1. Structural Properties of Monolayers 1−3[a]

					elemental ratio				
		monolayer composition	$d_{S(DTC)-S(thiol)}$ (Å)	AF[b]	O/N	C/N	$S_{(bound\ S)}/S_{(unbound\ S)}$[c]	S/Au[d]	MA (Å^2)[e]
1	protected	$C_{17}H_{24}NOS_3$	13.44	0.73	1.94	19.4	1.74 (2.38)	0.032	30.4
	deprotected	$C_{15}H_{22}NS_3$	13.36	0.73	0.59	15.7	1.61 (2.21)	0.033	29.5
2	protected	$C_{19}H_{28}NOS_3$	15.79	0.69	1.64	19.1	1.24 (1.80)	0.031	31.4
	deprotected	$C_{17}H_{26}NS_3$	15.96	0.68	0.74	18.4	1.57 (2.31)	0.033	29.5
3		$C_{15}H_{22}NS_2$	-	-	0.68	17.8	-	0.031	31.4

[a] The molecular length $d_{S(DTC)-S(thiol)}$ was determined from DFT gas-phase calculations. The attenuation factor AF was derived from the molecular length and the tilt angle of the molecules relative to the surface (28.6°), and was used for calculation of the corrected $S_{(bound\ S)}/S_{(unbound\ S)}$ ratios (corrected values in parentheses). Elemental ratios from XPS peak areas yielded the chemical composition for each self-assembled monolayer. The molecular area (MA) was obtained from the S/Au ratios by referencing to hexagonally close packed dodecanethiol monolayers. XP sensitivity factors were gained from the Kratos database and calibrated using known reference samples ($SF_{S\ 2p}$ = 0.668, $SF_{N\ 1s}$ = 0.477, $SF_{O\ 1s}$ = 0.780, $SF_{C\ 1s}$ = 0.330, $SF_{Au\ 4f}$ = 6.250). [b] Attenuation factor AF = $\exp(-x/\lambda)$, using an electron attenuation length (EAL) of λ = 3.7 nm, as computed with the program "NIST standard reference database 82". The monolayer thickness (x) was obtained from $x = \cos\alpha d_{S(DTC)-S(thiol)}$, where $d_{S(DTC)-S(thiol)}$ is the molecular length and α is the molecular tilt angle from the surface normal (α = 28.6°, see DFT calculations in the Supporting Information). [c] $S_{(bound\ S)}/S_{(unbound\ S)}$ is the ratio of the two S 2p peak areas with the $S_{2p3/2}$ components at ∼162 eV and ∼164 eV, respectively. Values in the parentheses were corrected by the attenuation factor (AF). [d] Ratio of the peak areas of bound S 2p (S) and of Au 4f (Au) divided by 2 to account for the presence of the two sulfur atoms in the dithiocarbamate group. [e] MA obtained from S/Au peak area ratios by reference to densely packed alkanethiol monolayers (S/Au ∼ 0.045, MA = 21.6 Å^2/molecule[39]).

(by ∼0.2 eV) than those found for thiolates on Au (162.1 eV for octanethiol monolayers). Dithiocarbamate monolayers of this kind have been studied previously,[18,19] and it is established that they bind to Au with both sulfur atoms in a bidentate configuration, providing outstanding contacts, both electrically and mechanically.[22] The molecular surface density of monolayer **3** (estimated via S 2p/Au 4f peak area ratios) is ∼0.7 times the density of a close packed dodecanethiol monolayer (Table 1), which can be rationalized in terms of a higher bulkiness of the dithiocarbamate anchor group. The chemical shift and molecular density were consistent with previous results obtained from [1,1′;4′,1″]terphenyl-4″-yl-methane-dithiocarbamate monolayers on Au.[22] Notably, the purity of the adsorbed monolayers is evident from C 1s/N 1s peak area ratios, which are very close to stoichiometric values for **3** as well as for **1** and **2** (see Table 1).

In case of rectifiers **1** and **2**, the situation is more complex, as there is a competition in the adsorption of the thiolate and dithiocarbamate moiety to the metal surface. To obtain a directional assembly of rectifiers **1** and **2** on Au, we took advantage of the fact that the rate constant for the molecular adsorption of acetyl-protected thiols on Au is 2 orders of magnitude lower than that for thiols on Au,[27,35] whereas the adsorption rate constant for dithiocarbamates is quite close to that of thiols (∼4 times lower compared to thiols).[26] These rate constants determine the orientational order of the resulting monolayers, as they make sure that rectifiers **1** and **2** attach to Au with the dithiocarbamate anchor group first. A stability test of the thioacetate group in basic dithiocarbamate solutions showed that the thioacetate moiety was stable during the assembly time; however, this stability decreases with the water content in solution (Supporting Information).

Upon self-assembly of monolayers of **1** and **2**, XPS allowed to distinguish between different sulfur species contributing to the S 2p spectrum. Furthermore, the oxygen O 1s signal indicated the presence of an acetyl protective group on the thiol moiety. In Figure 4, both the S 2p and the O 1s signals are shown for monolayers of **2** before and after deprotection with ammonium hydroxide, respectively. The monolayers feature two emission peaks at a BE of ∼162 eV and ∼164 eV (Figure 4a and Table 1 in Supporting Information). The peak at ∼162 eV is well-known to arise from thiolate[34] or dithiocarbamate[18] chemically bound to Au, whereas the peak at ∼164 eV is attributed either to unbound thiols[34,36] or to acetyl protected thiols.[37]

dx.doi.org/10.1021/ja110244j |J. Am. Chem. Soc. 2011, 133, 5921–5930

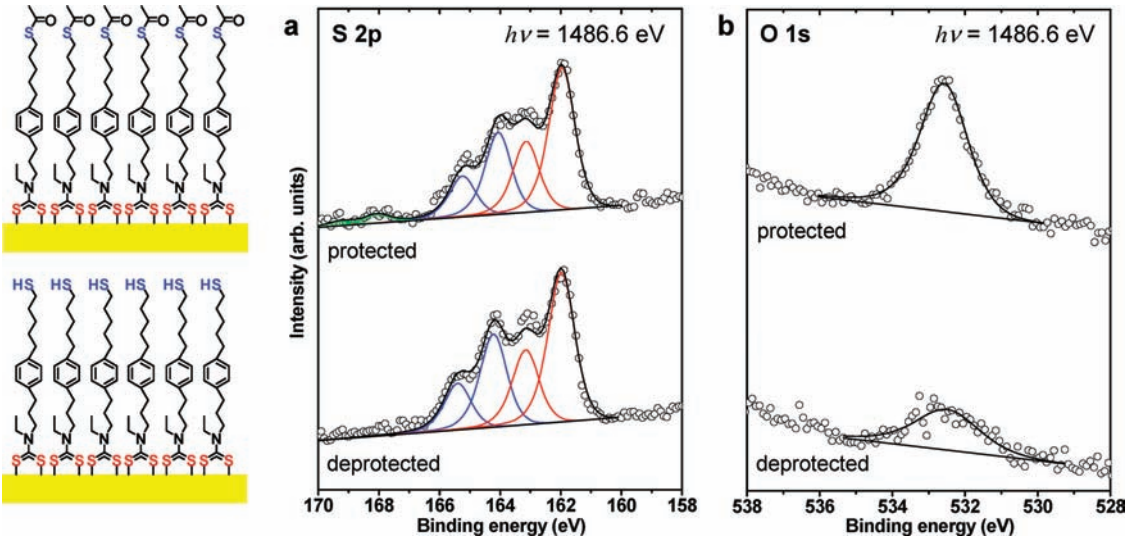

Figure 4. XP spectra of monolayer **2** on Au(111) acquired before deprotection (top) and after deprotection (bottom) in the S 2p (a) and the O 1s (b) spectral region. As shown in (a), the S $2p_{3/2}$ components at 161.95 and 164.04 eV were not affected by the treatment, whereas in (b), a clear reduction in the O 1s peak intensity at 532.6 eV was observed. Fit curves to the data are drawn in red and blue, corresponding to the two sulfur species shown in the left scheme. The sum of the fit curves and the linear background are drawn in black. The scheme on the left side shows the monolayer structure before and after deprotection.

To clarify the structure of monolayers **1** and **2**, a quantitative evaluation of XP signals was done, resulting in the figures listed in Table 1. From the S 2p/Au 4f peak area ratios, where only the bound sulfur component was taken into account, an average molecular density of ~0.73 times that of a dense dodecanethiol monolayer was obtained, which is very close to the density found for monolayer **3**. From DFT calculations utilizing experimental surface densities, an upright orientation of molecule **2** with an average tilt angle of ~28.6° toward the surface normal was derived (see Supporting Information for computational details).

On the basis of the two XP peaks S 2p(162 eV) and S 2p(164 eV), we obtained a ratio of their areas of A(162 eV)/A(164 eV) = 1.8−2.3. Here a correction factor that accounts for the photoelectron attenuation was applied (see Table 1 and Supporting Information). The result is in reasonable agreement with the expected relative amount of bound and unbound sulfur (A(bound)/A(unbound) = 2), when assuming an adsorption model as presented in Figure 2. According to this model, both sulfur atoms of the dithiocarbamate moiety attach to the substrate, whereas the protected thiol functionality is exposed to the surface. Unfortunately, when determining the ratio of the two areas, the instrumental error due to limited XPS resolution and partial overlap of the two components is ~10−15%; thus, we cannot exclude that a certain amount of rectifiers might attach to the surface through the thiolate or even bind in a "bridge" configuration. In any case, by exploiting the different adsorption rates of thioacetates and dithiocarbamates, a shorter assembly time (30−60 min) might help to reduce thiolate adsorption and thus provide a maximum yield of dithiocarbamate-linked molecules on Au.

Further supporting this scenario, the two protected monolayers show a consistent oxygen peak (O 1s at ~532.6 eV), indicative of the acetyl protective groups. The signal is strongly reduced upon deprotection. Note that a slight oxygen background (expected stoichiometry for **1** and **2**: O/N = 1), observed for all samples (including monolayer **3**), presumably indicates the presence of water adsorbed to the surface.

In contact angle measurements with deionized water, monolayer **3** showed values (~90°) that were fairly close to those from alkanethiols and dialkyldithiocarbamates (103−114°),[20] whereas monolayers **1** and **2** (~68° and ~74°, respectively) exhibited a higher polarity, characteristic of thiol-terminated surfaces (Supporting Information, Table 1).

From the above data, we conclude that the oriented assembly of target compounds **1** and **2**, as expected based on the slow rate of adsorption of thioacetates to Au, is the main feature of the studied monolayers. The orientational order is a prerequisite for the formation of rectifier-type junctions, in analogy to previous studies where the oriented growth could be achieved using monoacetylated dithiols.[38]

Deacetylation of the Thioacetate. The acetyl protection group was removed from the monolayer surface by treating the monolayer with ammonium hydroxide. Thiol and thioacetate exhibit the same chemical shift for the S 2p signal; thus, the deacetylation can only be monitored via changes in the O 1s signal. XP data showed that most of the oxygen was removed upon the treatment (Figure 4b), that is, its amount was decreased by about 1 oxygen atom/molecule (Table 1). Figure 4 shows that the treatment did not affect the monolayer structure as far as the bonding environment of the sulfur is concerned. Specifically, the BE of bound and unbound sulfur species, their relative peak areas and the molecular surface density (29−31 Å^2/molecule, see Table 1) were unchanged.

Further evidence for the deacetylation of the terminal thioester comes from PM-IRRAS, a technique which is highly specific to the detection of chemical bonds, as it relies on the analysis of vibrational modes that are excited by infrared radiation. The changes in the intensities of the asymmetric and symmetric in-plane C−H stretching modes of the methyl group, located at 2965 cm^{-1} ($\upsilon_a(CH_3)$) and 2879 cm^{-1} ($\upsilon_s(CH_3)$),[40,41] were used to monitor the presence of the methyl group in the acetyl moiety (Figure 5). Compounds **1** and **2** include two methyl groups, one of which is coordinated to the amine and the other one is part of the thioester functionality. In addition, there are

dx.doi.org/10.1021/ja110244j |J. Am. Chem. Soc. 2011, 133, 5921–5930

7 and 9 methylene groups for derivatives **1** and **2**, respectively, which appear in the asymmetric and symmetric C−H stretching modes at 2932 cm^{-1} ($\upsilon_a(CH_2)$) and 2854 cm^{-1} ($\upsilon_s(CH_2)$).[40] The position of the methylene peaks is consistent with monolayers existing in the liquid phase rather than in the crystalline phase.[41] This result was expected considering the short alkyl chains in molecules **1** and **2**. As shown in Figure 5, a strong decrease in the methyl $\upsilon_a(CH_3)$ signal intensity was observed for monolayer **2** upon treatment with ammonium hydroxide, thus, demonstrating the removal of the acetyl group from the thiol surface. The low intensities of the $\upsilon_s(CH_3)$ mode and of the thioacetyl C═O stretching vibration at 1680 cm^{-1} (not shown) can be explained by a parallel orientation of the acetyl S−C−C plane relative to the surface plane, because in this case both the $\upsilon_s(C{=}O)$ and $\upsilon_s(CH_3)$ transition dipoles are perpendicular to the surface normal (and thus not excited by the electrical field vector).[42]

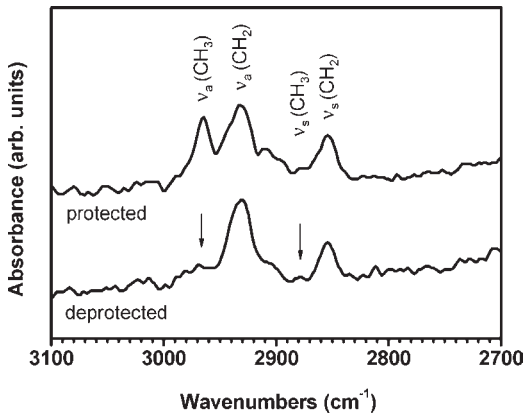

Figure 5. PM-IRRAS spectra of representative monolayer **2** in the 2700−3100 cm^{-1} region before and after removal of the acetyl protective group. The arrows indicate the position of the asymmetric and symmetric stretching modes of the methyl group at 2965 and 2879 cm^{-1}, respectively.

Au Nanoparticle Deposition. The metallization of the thiol-terminated surface was accomplished by incubation of the monolayer in a nanoparticle solution. This process was selected in view of the high sensitivity of thin self-assembled monolayers, which exclude any conventional thermal deposition of metals on them. During immersion of the monolayers in the NP solution, an exchange of the dodecylamine ligands linked to the NPs with the thiolate end groups at the monolayer surface occurred. Thus, a layer of NPs, chemically linked to the underlying monolayer, was formed. As dithiocarbamates **1** and **2** are completely insoluble in toluene, which is used as a solvent during nanoparticle incubation, a ligand exchange, that is, the desorption of dithiocarbamates from the surface with subsequent re-adsorption on the Au NP, can be excluded. Figure 6a shows an STM image of the template-stripped gold (TSG) surface modified with monolayer **1**, and Figures 6b and 7 show the same surface after deprotection and incubation with the Au NPs. Whereas in Figure 6a the characteristic features of a TSG surface are seen (despite the low roughness of Δh_{rms} ~0.3 nm, the grains of the polycrystalline Au surface appeared), in Figures 6b and 7 a close packed layer of Au clusters and NPs covers the surface. Here, we found peak-to-valley STM height differences of 6−20 nm, corresponding to the diameters of the Au clusters or of their agglomerates. The Au NPs were firmly attached to the surface because extensive rinsing of the sample in different solvents did not change the NP coverage. Control samples with monolayer **3**, lacking the thiol end group, were subjected to the same treatment, but did not show any difference in surface topography upon NP incubation (Figure 6c,d).

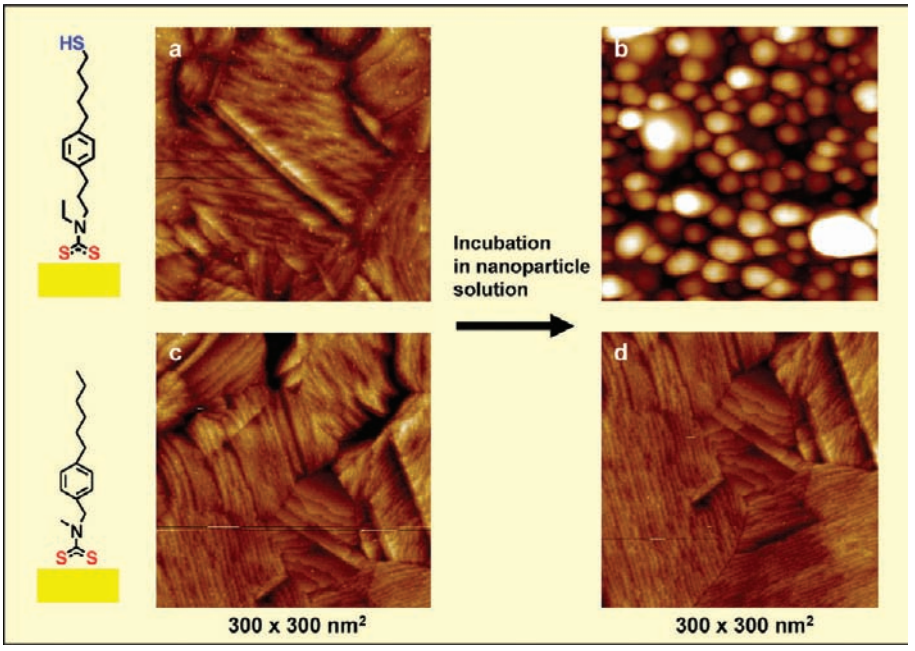

Figure 6. STM images of monolayer **1** on TSG before (a) and after (b) deprotection and NP incubation. (a) The rms roughness of the surface was ~0.3 nm, but it showed grains (100−200 nm in size) from the polycrystalline TSG surface. (b) After deprotection and NP incubation, the surface was densely covered with large gold clusters and NPs. Monolayer **3** on TSG before (c) and after (d) ammonium hydroxide treatment and NP incubation, demonstrating that the NPs did not bind to the surface. All images were acquired at a bias voltage of 400 mV and a tunneling current of 2 pA. The height scale was 3 nm for images a, c, and d and 20 nm for image b.

dx.doi.org/10.1021/ja110244j |*J. Am. Chem. Soc.* 2011, 133, 5921–5930

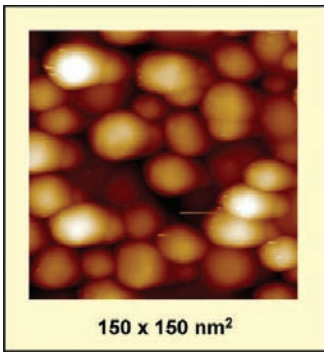

Figure 7. STM zoom image of monolayer **1** on TSG after deprotection and NP incubation. The image was acquired at a bias voltage of 400 mV and a tunneling current of 2 pA. The height scale was 15 nm.

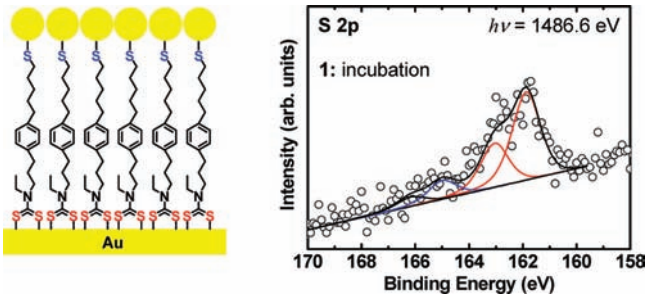

Figure 8. XP S 2p spectrum of monolayer **1** after deprotection and NP incubation. The unbound thiol component at ~164 eV almost vanished, showing that most of the terminal thiols in the monolayer reacted with the Au NPs (~162 eV). Fit curves to the data are drawn in red and blue, while the sum of the fit curves and the linear background are in black.

The efficiency of the metallization step, that is, the full chemisorption of the Au NPs to the thiol-terminated surface, was verified by XPS and showed the disappearance of one of the two thiol components in the S 2p spectral region (Figure 8). Although the total S 2p signal intensity was strongly attenuated by the presence of the Au NPs on top of the monolayer, a prevalent suppression of the S 2p component related to unbound sulfur at ~164 eV could be observed (see Figure 4 for comparison).

Thus, most of the thiols at the surface are converted to thiolates upon reaction with the Au NPs in solution, and a thin metal layer is formed at the monolayer surface. The whole process delivers a metal−molecule−metal junction that is intrinsically asymmetric due to the choice of the two different anchor groups employed for molecular self-assembly.

Electrical Characterization. An alternative approach for contacting monolayers is the deposition of a highly conducting polymeric interlayer between the monolayer of interest and, for example, a thermally evaporated top electrode. This technique enabled the measurement of large area molecular junctions with diameters up to 100 μm.[13] We used monolayers as described in the section "Deacetylation of the Thioacetate" and deposited a poly(3,4-ethylene-dioxythiophene):poly(4-styrenesulphonic-acid) (PEDOT:PSS) film on these surfaces for further electrical characterization with a hanging Hg-drop apparatus (see Experimental Section). Because of the polar character of the water-soluble PEDOT:PSS suspension, these films are highly adhesive to the thiol end groups of the monolayers. PEDOT:PSS was spin coated onto monolayers of **1** and **2**, forming polymeric films with a homogeneous thickness of about 100 nm. The current−voltage characteristics were acquired in the bias range from −1 to 1 V, and measurements comparing curves from **1** and **2** with data from alkanedithiol monolayers having different chain length (1,8-octyldithiol (ODT) and 1,12-dodecanedithiol (DDT)) allowed us to determine the conductance per unit area of monolayers of **1** and **2**. The curves were very reproducible on different samples and positions. The average current densities in Figure 9

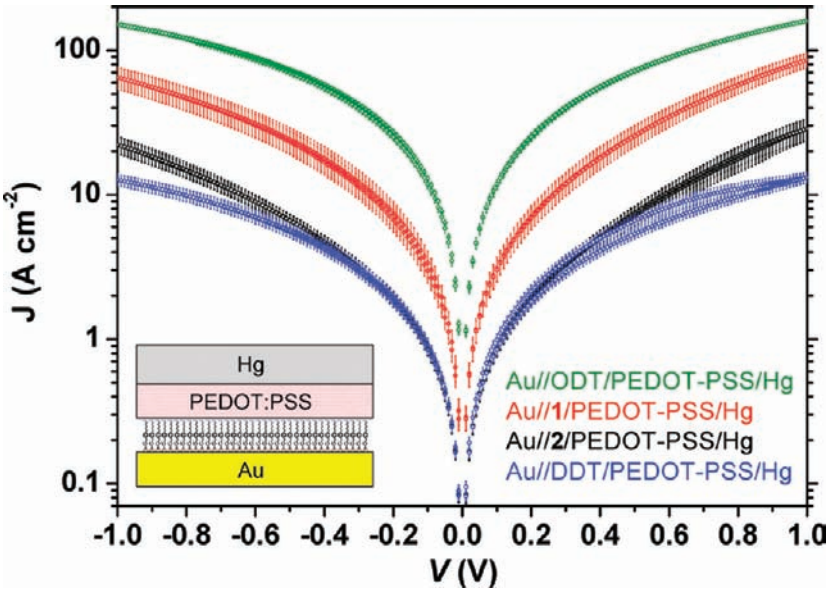

Figure 9. Average current density versus bias voltage for monolayer junctions of **1** and **2** having the structure Au//Monolayer/PEDOT:PSS/Hg. The curves are compared with data from ODT and DDT in analog devices. At a bias of 1 V, the current densities for DDT:**2**:**1**:ODT follow the ratio 1:3:7:13. The error bars indicate the standard deviation for the measured curves. The scans are acquired from 0 to 1 V, down to −1 V and back to 0 V. Both scan directions are shown in the graph. The individual scans in a linear representation are shown in the Supporting Information (Figures S4 and S5).

dx.doi.org/10.1021/ja110244j |*J. Am. Chem. Soc.* 2011, 133, 5921–5930

show that at a bias of 1 V the conductance of a monolayer of **2** is 3.1 times lower than that of a monolayer of **1** and 2.2 times higher than that of a DDT monolayer. The ratio in the conductance of ODT and DDT monolayers was 13. These proportions in the conductance of the layers are in good agreement with values obtained if a simple tunnelling barrier model[5,43] with an attenuation factor of $\beta \sim 0.5/\text{Å}$ is applied. Referred to the molecular structure (see Figure 1), this means that the current density scales exponentially with the length of the barrier x,

$$J \propto \exp(-\beta x)$$

that is, with the number of aliphatic bonds within the molecular junction. The current densities for ODT and DDT junctions are in excellent agreement with values reported by de Boer et al.,[13] even though in our case a Hg drop electrode rather than a thermally evaporated Au contact was employed. Also the measured tunnelling decay constant, even though lower than reported with other experimental test beds, is very close to previous results gained with monolayer/PEDOT:PSS junctions.[13]

Interestingly, above a bias of ~0.4 V, the rise in current density for **1** and **2** is significantly more pronounced than for alkanedithiols. This is probably caused by the frontier orbitals of the phenyl ring in molecular rectifiers **1** and **2**, which above a certain bias voltage are aligned with the Fermi level of one of the electrodes and thus become accessible for resonant tunnelling. In addition, at a bias of at 1 V, for both rectifiers a moderate rectification (rectification ratio = 1.32) is found. This effect, observed for the first time in monolayer/polymer type junctions, does not show up in alkanedithiol junctions that are intrinsically symmetric. Hence, the observed rectification can be attributed to the asymmetry of the monolayer junctions consisting of the oriented self-assembled rectifiers **1** and **2**.

In summary, the presented electrical data show a clear signature from the molecular layers and confirm that the current density reflects the nature of the molecules in the respective junction, both concerning molecular length and structure. It also shows that, as for ODT and DDT monolayers, the packing density and orientation of rectifiers **1** and **2** is sufficiently well-defined to avoid electrical shorts in the molecular junctions. However, it should be mentioned that polymeric interlayers do not allow a systematic study of molecular rectification since the electrical contact with the terminal thiol groups is not well understood, as it is for thiolate−Au interfaces. For a quantitative investigation, identical metal electrodes on both sides of the junction are required, and single-molecule measurements are currently ongoing to correlate theoretical predictions with experimental rectification ratios.

CONCLUSIONS

The fabrication of metal−molecule−metal junctions consisting of monolayers of aligned, self-assembled rectifier candidates has been reported in this study. The oriented growth of these rectifiers has been achieved by making use of the different adsorption rate constants of dithiocarbamates and acetyl protected thiols on Au surfaces. The critical top electrode deposition was demonstrated both by nanoparticle incubation and by formation of conducting polymeric films. Electrical measurements with large area polymeric junctions reflect the conductance of the molecular layers, demonstrating the feasibility of monolayer-based junctions. The presented method is a simple and reproducible procedure for the realization of devices with an asymmetric electrode−monolayer−electrode structure, an issue of high relevance to obtain diodes in molecular electronics.

EXPERIMENTAL SECTION

Monolayer Preparation. For XPS, FT-IR, STM, and contact angle characterization, template-stripped gold (TSG) surfaces were prepared using known procedures.[44] In short, Au was deposited by thermal evaporation (100 nm) onto a polished silicon wafer (Si-Mat GmbH). A glass slide covered with epoxy glue (EPO-TEC 353, Polytec) was then deposited on the Au surface. Subsequently, the glue was cross-linked at 150 °C (for 1 h). The TSG surface was formed by stripping the Au on the glass from the silicon wafer with the aid of a razor, yielding substrates with a rms roughness of 0.3 nm, as observed by atomic force microscopy. The self-assembled monolayers were prepared in an argon environment (glovebox) by immersion of the freshly cleaved TSG samples into 0.2 mM solutions of dithiocarbamate salts **1**, **2**, or **3** in absolute ethanol for 18−24 h. Such a long assembly time was chosen because a long exposure of Au surfaces to thiols or dithiocarbamates is known to provide denser, higher quality monolayers. However, we also tested the assembly of dithiocarbamates for times as short as 1 h, without significant loss in monolayer density as far as XPS spectra are concerned. A shorter soaking time probably slightly reduces the fraction of molecules linked to Au with the thiol moiety. After self-assembly, all samples were thoroughly rinsed with absolute ethanol, blown dry with argon, and immediately used for characterization. The samples were then transferred for XPS analysis in argon filled containers. To avoid oxidation, all solvents used for monolayer preparation and processing (ethanol and methanol) were saturated with argon before use.

Deacetylation and Au Nanoparticle Incubation. The acetyl protective groups were removed by exposing the monolayers of **1** and **2** to an ethanolic solution of ammonium hydroxide (0.52 M) for 12 h. The resulting samples were thoroughly rinsed with ethanol and immersed into a freshly prepared solution of dodecylamine-stabilized Au nanoparticles[45] (average particle diameter: 4 nm) in toluene for 18 h. The concentration of this nanoparticle solution was adjusted to an absorbance of 0.4 at the maximum of the plasmon absorption band (λ_{max} = 514 nm, 2 mm path length). After incubation, excess nanoparticles were removed by rinsing the samples with toluene and ethanol and drying them in a stream of N_2.

UV−Vis and Infrared Spectroscopy. UV/vis absorption spectra were recorded using a Varian Cary 50 scan spectrophotometer using a cell path length of 1 cm. Polarization modulation infrared reflection−absorption spectroscopy (PM-IRRAS) data were acquired with a Bruker Vertex 70 spectrometer equipped with a PMA50 module including a nitrogen cooled mercury−cadmium−telluride (MCT) detector and a ZnSe photoelastic modulator. The IR beam was set at 80° incident to the TSG surface, and the spectra were collected over 15 min at a resolution of 4 cm^{-1}.

Contact Angle Goniometry. To determine the surface energy of the monolayer, contact angle measurements were done with a KSV CAM 100 at room temperature. A drop of deionized water from a Millipore system (18.2 MΩ·cm) was dispensed on the surface after rinsing it with ethanol and drying it in nitrogen.

X-ray Photoelectron Spectroscopy (XPS). High-resolution XPS spectra were recorded with a Kratos Axis Ultra instrument using an Al Kα (1486.6 eV) source operated at 15 kV and 180 W. With an X-ray monochromator and a pass energy of 40 eV for the analyzer, an instrumental energy resolution of 0.5 eV was achieved. A survey spectrum and high resolution spectra of the S 2p, C 1s, N 1s, O 1s and Au 4f regions were acquired. The binding energies were calibrated against the Au $4f_{7/2}$ core-level peak at 84 eV. The spectra were fitted using Voigt functions with a 50/50 Lorentz/Gaussian ratio and a linear background. The line shape parameters were determined by

least-square fitting to carbon and sulfur core-level signals of known alkanethiol reference samples. The S 2p spectrum, consisting of the two components S $2p_{3/2}$ and S $2p_{1/2}$ with a fixed separation of 1.18 eV, was fitted with a relative ratio of 2/1 for the S $2p_{3/2}$/S $2p_{1/2}$ areas. The molecular surface density was obtained from the relative S/Au signal intensity by consideration of the bound S 2p component only (~162 eV), which allowed a direct comparison with the surface density of other dithiocarbamate or thiol derivatives. The S/Au intensity ratio is independent on the specific molecular structure of various organosulfur compounds that are chemically linked to Au, thus a reliable indicator for molecular densities.

Scanning Tunneling Microscopy (STM). The structural properties of the modified TSG surfaces were characterized using a scanning tunneling microscope (Multimode Nanoscope IIIa, Digital Instruments) equipped with a low current amplifier. Self-cut Pt/Ir (80/20) tips were used as a probe. The STM scans were recorded in constant-current mode under ambient conditions at room temperature.

Electrical Measurements. For sample preparation, the self-assembly of rectifier molecules and subsequent deacetylation were carried out following the same procedure as described above. The monolayers of 1,8-octyldithiol and 1,12-dodecanedithiol were prepared by immersion of the TSG substrates into 3 mM ethanolic solutions of the dithiols for 36 h.[46] After monolayer preparation, the substrates were rinsed intensely with ethanol. A poly(3,4-ethylenedioxythiophene):poly(4-styrenesulphonic-acid) (PEDOT:PSS) solution was prepared by diluting 0.25 mL of the water-based source suspension (Clevios FE, H.C. Starck GmbH & Co.) with 0.35 mL of methanol and by subsequent filtration through a nylon filter having a pore size of 0.1 μm. The PEDOT:PSS solution was then spin coated onto the TSG substrates at 1500 rpm for 50 s and dried in a vacuum chamber, resulting in a polymer film with a thickness of ~100 nm. For electrical characterization, a home-built Hg-drop setup with a Hamilton syringe as Hg-dispenser was employed. Technical details about the experimental setup are reported elsewhere.[22] The measurements were carried out under ambient conditions, that is, the Hg droplet was extruded and suspended in air above the sample. Subsequently, the surface was approached using a piezo-table until a large area contact (0.39 ± 0.03 μm in diameter) between sample and Hg droplet was established. The contact of the Hg droplet with the sample was monitored from side-view using a CCD-camera, and based on the junction diameter, the contact area was determined. Current−voltage curves were acquired on 2 different samples and on 6 positions in total. For each position, a series of 5 curves was recorded with a maximum bias value at 0.1, 0.2, 0.5, 0.6, and 1 V. The data was acquired using a voltage ramp with a bin size of 10 mV and an elapsed time between steps of 0.1 s. Averaged curves were created from 6 single scans on 2 different samples. The Hg electrode was on ground and the bias applied to the bottom TSG electrode. Current densities were obtained by normalizing the currents with the contact area of the Hg droplet on the sample.

■ ASSOCIATED CONTENT

Supporting Information. Synthesis procedures and ^{1}H NMR spectra of compounds **1** and **3** and the intermediates, molecular modeling results, XPS and electrical data. This material is available free of charge via the Internet at http://pubs.acs.org.

■ AUTHOR INFORMATION

Corresponding Author
Florian.vonWrochem@eu.sony.com

■ ACKNOWLEDGMENT

We thank Dr. Nadja Krasteva and Dr. Yvonne Joseph for providing Au nanoparticles and Dr. Armin Gembus from Bruker Optics for the acquisition of PM-IRRAS spectra.

■ REFERENCES

(1) 2009 Semiconductor Industry Association, International Technology Roadmap for Semiconductors 2009 Edition, Emerging Research Devices; http://www.itrs.net/Links/2009ITRS/Home2009.htm. 2009.
(2) Carroll, R. L.; Gorman, C. B. *Angew. Chem., Int.Ed.* **2002**, *41*, 4379–4400.
(3) Joachim, C.; Gimzewski, J. K.; Aviram, A. *Nature* **2000**, *408*, 541–548.
(4) Tao, N. J. *Nat. Nanotechnol.* **2006**, *1*, 173–181.
(5) Akkerman, H. B.; de Boer, B. *J. Phys.: Condens. Matter* **2008**, *20*, 013001.
(6) Campbell Scott, J.; Bozano, L. D. *Adv. Mater.* **2007**, *19*, 1452–1463.
(7) Green, J. E.; Choi, J. W.; Boukai, A.; Bunimovich, Y.; Johnston-Halperin, E.; Delonno, E.; Luo, Y.; Sheriff, B. A.; Xu, K.; Shin, Y. S.; Tseng, H.-R.; Stoddard, F.; Heath, J. R. *Nature* **2007**, *445*, 441–444.
(8) Snider, G. S.; Williams, R. S. *Nanotechnology* **2007**, 18.
(9) Aviram, A.; Ratner, M. A. *Chem. Phys. Lett.* **1974**, *29*, 277–283.
(10) Metzger, R. M. *Chem. Rev.* **2003**, *103*, 3803–3834.
(11) Kornilovitch, P. E.; Bratkovsky, A. M.; Williams, R. S. *Phys. Rev. B* **2002**, *66*, 165436−1–165436−11.
(12) Love, J. C.; Estroff, L. A.; Kriebel, J. K.; Nuzzo, R. G.; Whitesides, G. M. *Chem. Rev.* **2005**, *105*, 1103–1169.
(13) Akkerman, H. B.; Blom, P. W. M.; de Leeuw, D. M.; de Boer, B. *Nature* **2006**, *441*, 69–72.
(14) Jiang, P.; Morales, G. M.; You, W.; Yu, L. P. *Angew.Chem., Int. Ed.* **2004**, *43*, 4471–4475.
(15) Yu, C. J.; Chong, Y.; Kayyem, J. F.; Gozin, M. *J. Org. Chem.* **1999**, *64*, 2070–2079.
(16) Pollack, S. K.; Naciri, J.; Mastrangelo, J.; Patterson, C. H.; Torres, J.; Moore, M.; Shashidhar, R.; Kushmerick, J. G. *Langmuir* **2004**, *20*, 1838–1842.
(17) Wessels, J. M.; Nothofer, H. G.; Ford, W. E.; von Wrochem, F.; Scholz, F.; Vossmeyer, T.; Schroedter, A.; Weller, H.; Yasuda, A. *J. Am. Chem. Soc.* **2004**, *126*, 3349–3356.
(18) Morf, P.; Raimondi, F.; Nothofer, H.-G.; Schnyder, B.; Yasuda, A.; Wessels, J. M.; Jung, T. A. *Langmuir* **2006**, *22*, 658–663.
(19) Zhao, Y.; Pérez-Segarra, W.; Shi, Q.; Wei, A. *J. Am. Chem. Soc.* **2005**, *127*, 7328–7329.
(20) Weinstein, R. D.; Richards, J.; Thai, S. D.; Omiatek, D. M.; Bessel, C. A.; Faulkner, C. J.; Othman, S.; Jennings, G. K. *Langmuir* **2007**, *23*, 2887–2891.
(21) Cao, R.; Diaz, A.; Cao, R.; Otero, A.; Cea, R.; Rodriguez-Arguelles, M. C.; Serra, C. *J. Am. Chem. Soc.* **2007**, *129*, 6927–6930.
(22) von Wrochem, F.; Gao, D.; Scholz, F.; Nothofer, H. G.; Nelles, G.; Wessels, J. M. *Nat. Nanotechnol.* **2010**, *5*, 618–624.
(23) Li, Z.; Kosov, D. S. *J. Phys. Chem. B* **2006**, *110*, 9893–9898.
(24) Loertscher, E.; Gao, D.; Schwarz, F.; Gotsmann, B.; Ford, W. E.; von Wrochem, F.; Riel, H. Unpublished results 2011.
(25) McCubbin, Q. J.; Stoddart, F. J.; Welton, T.; White, A. J. P.; Williams, D. J. *Inorg. Chem.* **1998**, *37*, 3753–3758.
(26) Zhu, H.; Coleman, D. M.; Dehen, C. J.; Geisler, I. M.; Zemlyanov, D.; Chmielewski, J.; Simpson, G. J.; Wei, A. *Langmuir* **2008**, *24*, 8660–8666.
(27) Schwartz, D. K. *Annu. Rev. Phys. Chem.* **2001**, *52*, 107–137.
(28) Lane, C. F. *Chem. Rev.* **1976**, *76*, 773–799.
(29) Kiuchi, M.; Adachi, K.; Kohara, T.; Minoguchi, M.; Hanano, T.; Aoki, Y.; Mishina, T.; Arita, M.; Nakao, N.; Ohtsuki, M.; Hoshino, Y.; Teshima, K.; Chiba, K.; Sasaki, S.; Fujita, T. *J. Med. Chem.* **2000**, *43*, 2946–2961.
(30) Brown, H. C.; Choi, Y. M.; Narasimhan, S. *J. Org. Chem.* **1982**, *47*, 3153–3163.

(31) Zheng, T.-C.; Burkart, M.; Richardson, D. E. *Tetrahedron Lett.* **1999**, *40*, 603–606.
(32) Plenio, H.; Hermann, J.; Diodone, R. *Inorg. Chem.* **1997**, *36*, 5722–5729.
(33) Bergeron, R. J.; McManis, J. S. *J. Org. Chem.* **1988**, *53*, 3108–3111.
(34) Laibinis, P. E.; Whitesides, G. M.; Allara, D. L.; Tao, Y.-T.; Parikh, A. N.; Nuzzo, R. G. *J. Am. Chem. Soc.* **1991**, *113*, 7152–7167.
(35) Lau, K. H. A.; Huang, C.; Yakovlev, N.; Chen, Z. K.; O'Shea, S. J. *Langmuir* **2006**, *22*, 2968–2971.
(36) Nuzzo, R. G.; Zegarski, R.; Dubois, L. H. *J. Am. Chem. Soc.* **1987**, *109*, 733–740.
(37) Tour, J. M.; Jones, L., II; Pearson, D. J.; Lamba, J. J. S.; Burgin, T. P.; Whitesides, G. M.; Allara, D. L.; Parikh, A. N.; Atre, S. V. *J. Am. Chem. Soc.* **1995**, *117*, 9529–9534.
(38) Niklewski, A.; Azzam, W.; Strunskus, T.; Fischer, R. A.; Woll, C. *Langmuir* **2004**, *20*, 8620–8624.
(39) Schreiber, F. *Prog. Surf. Sci.* **2000**, *65*, 151–256.
(40) Allara, D. L.; Swalen, J. D. *J. Phys. Chem.* **1982**, *86*, 2700–2704.
(41) Porter, M. D.; Bright, T. B.; Allara, D. L.; Chidsey, C. E. D. *J. Am. Chem. Soc.* **1987**, *109*, 3559–3568.
(42) Ulman, A. *An Introducton to Ultrathin Organic Films*; Academic Press: San Diego, CA, 1991.
(43) Wang, W.; Lee, T.; Reed, M. A. *Phys. Rev. B* **2003**, *68*, 035416-1–035416-7.
(44) Naumann, R.; Schiller, S. M.; Giess, F.; Grohe, B.; Hartman, K. B.; Karcher, I.; Koper, I.; Lubben, J.; Vasilev, K.; Knoll, W. *Langmuir* **2003**, *19*, 5435–5443.
(45) Leff, D. V.; Brandt, L.; Heath, J. R. *Langmuir* **1996**, *12*, 4723–4730.
(46) Akkerman, H. B.; Kronemeijer, A. J.; van Hal, P. A.; de Leeuw, D. M.; Blom, P. W. M.; de Boer, B. *Small* **2008**, *4*, 100–104.